ACS Catalysis

RESEARCH ARTICLE

pubs.acs.org/acscatalysis

Aerobic Oxidation of Hydrocarbons Catalyzed by Mn-Doped Nanoporous Aluminophosphates (IV): Regeneration Mechanism

Luis Gómez-Hortigüela,* Furio Corà,* and C. Richard A. Catlow

Department of Chemistry, 20 Gordon Street, University College London, WC1H 0AJ London, United Kingdom

Supporting Information

ABSTRACT: Electronic structure methods based on periodic DFT with hybrid-exchange functionals are applied to study the reaction mechanism of the aerobic oxidation of hydrocarbons catalyzed by Mn-doped nanoporous aluminophosphates. Here, we focus on the *regeneration* of the active sites that closes the oxidation cycle. At this stage, the catalyst pores are accumulated with CH_3CH_2OOH (hydroperoxide) and $Mn^{III}\cdots OOCH_2CH_3$ complexes resulting from the propagation reactions. CH_3CH_2OOH intermediates can only be decomposed into the oxidation products by Mn^{II} sites; thus, a reaction pathway in which Mn sites in $Mn^{III}\cdots OOCH_2CH_3$ are reduced is essential for the oxidation cycle to proceed. We demonstrate that two different regeneration mechanisms take place at different times of the oxidation reaction: at the beginning, $Mn^{III}\cdots OOCH_2CH_3$ complexes are transformed into a molecule of aldehyde and $Mn^{III}\cdots OH$ complexes by an intramolecular H transfer from the methylene C to the terminal O in the peroxo radical in a slow process that requires a high activation energy of 141 kJ/mol. Mn sites in $Mn^{III}\cdots OH$ can then be regenerated by a H-transfer from a new hydrocarbon molecule to a framework O nearest neighbor to Mn, followed by coupling between the resulting alkyl radical and the OH ligand to give a molecule of ethanol and Mn^{II} sites. At later stages of the oxidation, when alcohol molecules are accumulated within the pores of the catalyst, Mn sites in $Mn^{III}\cdots OOCH_2CH_3$ can be regenerated by a more favorable mechanism with a double H-abstraction from the alcohol. First, a H atom in the methylene C of CH_3CH_2OH is transferred to the CH_3CH_2OO ligand to give CH_3CH_2OOH and $CH_3CH\cdot OH$ radicals, followed by H transfer from this radical to a framework O to yield finally a molecule of aldehyde and Mn^{II} sites. The occurrence of alternative regeneration mechanisms along the oxidation reaction explains the variation of the alcohol-to-aldehyde ratio observed experimentally as a function of the reaction time.

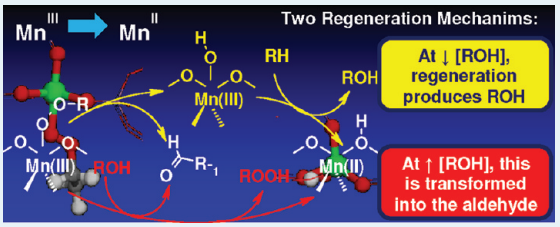

KEYWORDS: oxidation, heterogeneous catalysis, nanoporous aluminophosphates, zeolites, regeneration, aerobic, reaction mechanism

INTRODUCTION

Selective oxyfunctionalizations of saturated hydrocarbons with environmentally friendly oxidants such as molecular oxygen represent a major challenge in contemporary catalytic chemistry. Such oxidations are achieved efficiently and at low temperature by some enzymes; however, the high cost and low stability of enzymes limit their use on an industrial scale. Several investigations aimed at finding alternative synthetic pathways based on heterogeneous catalysts that are able to use molecular oxygen as the oxy-functionalizer agent have indicated that doped crystalline nanoporous aluminophosphate materials (AlPOs) are promising candidates for this goal.[1] Of particular importance are those materials in which tetrahedral Al is replaced by transition metal cations, such as Co, Mn, and Fe, to produce MeAPO materials.[2−9] A large body of work has been dedicated to study the catalytic activity of MeAPOs in oxidation reactions;[10−21] however, the exact mechanism of these catalytic oxidations is not known in its entirety, partly because of the complexity of the reaction pathways and intermediates involved as well as their short lifetime, which is unsuitable for in situ characterization. Experimental evidence indicates clearly that the aerobic oxidation of hydrocarbons catalyzed by MeAPOs occurs via a free-radical mechanism.[8,15]

The aerobic oxidation of cyclohexane catalyzed by MnAPO-5, a Mn-doped aluminophosphate with AFI structure, has been the subject of in-depth experimental studies by Iglesia and coworkers.[15] They proposed for this oxidation a reaction scheme that is based on extensive spectroscopic and isotopic labeling techniques. However, many of the intermediates involved are postulated because they cannot be directly detected. Complementary information can be gained from computational electronic-structure methods, such as those based on periodic density functional theory that are at the basis of the current work.

In a previous communication, we reported a computational analysis of the complete reaction mechanism for the aerobic oxidation of ethane catalyzed by Mn-doped AlPO-5,[22] in which the catalytic cycle has been divided into four subsequent stages named *preactivation*, hydroperoxide *decomposition*, *propagation*, and *regeneration*. Each stage is examined in greater detail in a series of publications,[23−25] which concludes with the present paper in which we examine the catalyst regeneration. The two possible oxidation states of Mn in AlPOs, Mn^{II}, and Mn^{III}, are

Received: August 2, 2011
Revised: September 14, 2011
Published: September 16, 2011

dx.doi.org/10.1021/cs200402b | ACS Catal. 2011, 1, 1475–1486

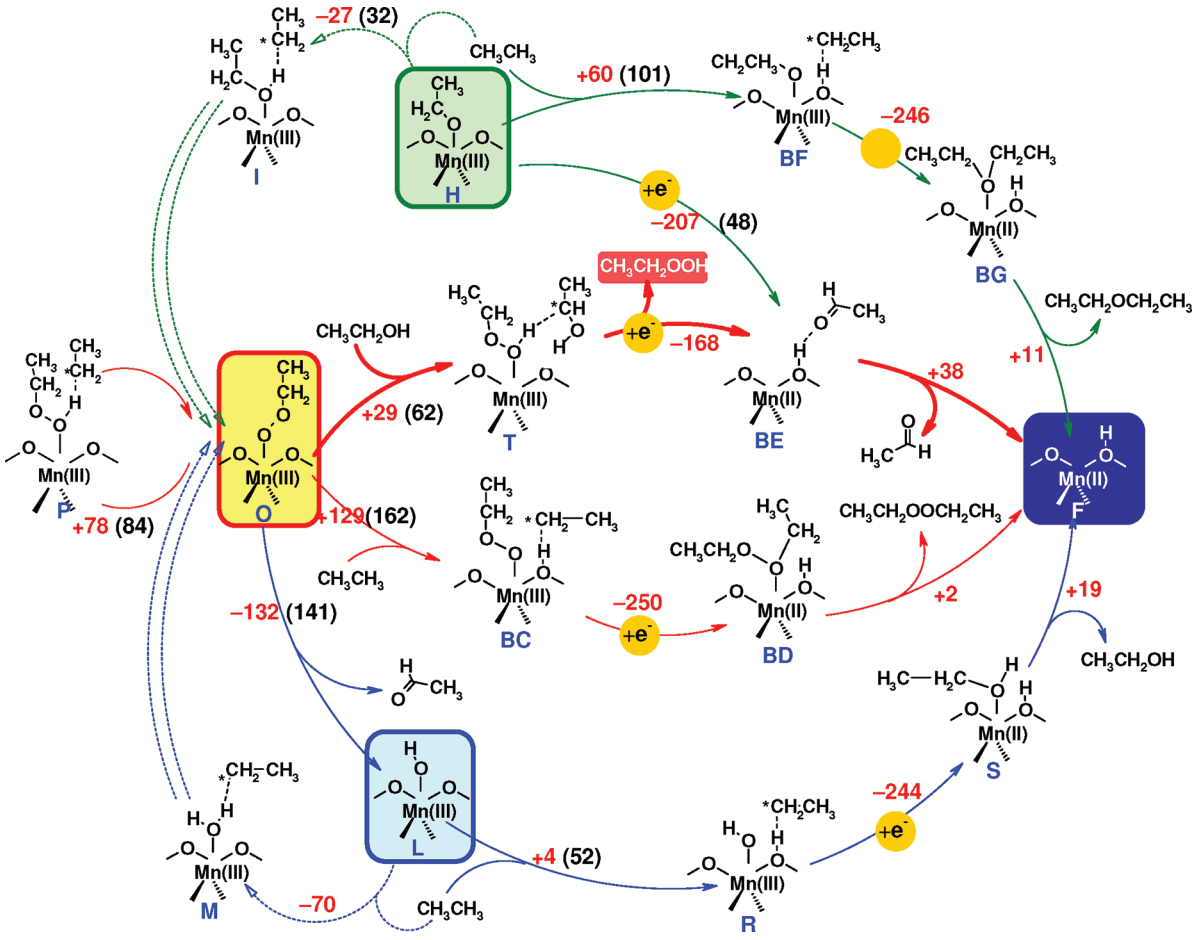

Figure 1. Scheme of the regeneration reactions studied in this work. Dashed arrows indicate steps that are part of the propagation cycle. Enthalpies (in red) and activation energies (if any, in black and between brackets) are given in kJ/mol.

both involved in the main catalytic cycle. In the initial *preactivation* step, the Mn^{III} sites present in the calcined catalyst are transformed into Mn^{II}- and Mn^{III}-peroxo complexes, from which the proper catalytic cycle proceeds.[23] Mn^{III}-peroxo complexes are responsible for the production of hydroperoxide intermediates (CH_3CH_2OOH), which can be decomposed only by the action of reduced Mn^{II} sites. The *decomposition* of CH_3CH_2-OOH can take place through two alternative mechanistic routes, that produce $Mn^{III}\cdots OCH_2CH_3$ and H_2O or $Mn^{III}\cdots OH$ and CH_3CH_2OH, depending on the stereochemistry of the CH_3CH_2OOH adsorption on the Mn^{II} active site.[24] Subsequent *propagation* reactions take place from the $Mn^{III}\cdots OX$ complexes; the radical nature of the oxo-type ligands activates homolytic H-abstraction from new hydrocarbon molecules (RH), generating a closed shell HOX molecule and an alkyl radical R·, followed by O_2 additions to the alkyl radical and desorption of HOX from the Mn^{III} site.[25] The peroxo radical ROO· eventually adsorbs onto Mn^{III} to yield $Mn^{III}\cdots OOCH_2CH_3$ complexes, from which new propagation reactions can occur, leading to the production of a further hydroperoxide intermediate and, again, $Mn^{III}\cdots$ $OOCH_2CH_3$ complexes, closing a hydroperoxide production subcycle.[25] However, these hydroperoxide molecules can be decomposed only through reduced Mn^{II} active sites, whereas in the propagation stage of the catalytic cycle, all Mn sites are in the oxidized 3+ state. Therefore, a reaction pathway that accounts for the reduction of Mn^{III} sites is essential to close the oxidation reaction cycle; we refer to this pathway as the *regeneration* mechanism. In this work, we focus on the different reaction routes available for such a regeneration of the active sites, starting from the Mn species produced during the propagation reactions.

The computational methodology applied here is the same as discussed in refs 23 and 24, to which the reader is referred to for all details. Ethane (CH_3CH_3) and the Mn-doped AFI structure (MnAPO-5) have been used as models for the hydrocarbon and the catalyst, respectively.The Mn-doped AFI framework is described with periodic boundary conditions, using one crystallographic unit cell (72 atoms) without symmetry, in which one Mn ion replaces Al in a tetrahedral position. We have performed density functional theory (DFT) calculations, as implemented in the program CRYSTAL,[26] using the hybrid-exchange functional B3LYP. Selected reaction steps have also been studied using the B3LYP+D functional, including the empirical correction for dispersion proposed by Grimme.[27,28] Since both reagent and product molecules are contained in the zeolitic pores, we found the dispersion correction to be negligible.[23,24] This is particularly true for the chemical transformations with the highest activation energies, which involve only the transfer of one H atom between reagent molecules. For this reason, only uncorrected B3LYP results are discussed in this paper. At each elementary step, constrained geometry optimizations were performed scanning a chosen reaction coordinate and relaxing all other internal coordinates. This methodology allowed us to obtain the energy

dx.doi.org/10.1021/cs200402b |*ACS Catal.* 2011, 1, 1475–1486

profile for each elementary step along the selected reaction coordinate, from which the transition states and the corresponding activation energies were identified. The approximate transition state (TS) identified in this constrained search was very close to that obtained using second-derivative-based methods, both in geometry (to within the step size chosen) and energy (usually less than 4 kJ/mol). Fully optimized configurations for reactants and products were used to find reaction enthalpies for each elementary step.

RESULTS

As in all our studies of this catalytic reaction, the labeling used for each intermediate and transition state in the reaction cycle is the same as introduced in reference 22; a full diagram of the reaction cycle is given in the Supporting Information (Figure 1-SI). In previous publications, we studied in detail (i) the preactivation of the initial Mn^{III}-AFI catalysts in the presence of O_2 and hydrocarbon (CH_3CH_3) to give the reduced form of the catalyst (Mn^{II}-AFI, **F**), the hydroperoxide intermediate (CH_3CH_2OOH) and a complex between Mn^{III} and a peroxo radical ($Mn^{III}\cdots OOCH_2CH_3$, **O**);[23] (ii) the decomposition of the hydroperoxide intermediate CH_3CH_2OOH assisted by Mn^{II} to give complexes of Mn^{III} with alkoxy ($CH_3CH_2O\cdot$) or hydroxy ($HO\cdot$) radicals ($Mn^{III}\cdots OCH_2CH_3$ (**H**) and $Mn^{III}\cdots OH$ (**L**), respectively);[24] and (iii) the propagation reactions, in which new hydrocarbon molecules were activated by Mn^{III} complexes with O-based ligands ($Mn^{III}\cdots OCH_2CH_3$ (**H**), $Mn^{III}\cdots OH$ (**L**) and $Mn^{III}\cdots OOCH_2CH_3$ (**O**)) through H transfer, followed by O_2 addition reactions and ligand desorptions.[25]

These propagation reactions involve only Mn^{III} sites—no redox process takes place at the Mn active site—and lead to the production of ethanol (CH_3CH_2OH), water (H_2O), and further hydroperoxide intermediate (CH_3CH_2OOH). However, these hydroperoxide molecules can be transformed into the oxidation products only by means of Mn^{II} sites, which are not present in the propagation stage of the oxidation reaction; therefore, these Mn sites need to be recovered for the oxidation cycle to proceed. In the present study, we focus on the last step of the oxidation mechanism, which involves the reduction of the Mn^{III} sites of complexes $Mn^{III}\cdots OCH_2CH_3$ (**H**), $Mn^{III}\cdots OH$ (**L**), and $Mn^{III}\cdots OOCH_2CH_3$ (**O**) to Mn^{II} in a process that we refer to as catalyst *regeneration*. The Mn^{II} sites, in turn, enable the decomposition of the hydroperoxide molecules into the Mn^{III} complexes (**H** and **L**), closing the reaction cycle. Hereafter, the ethyl chain CH_3CH_2 will be denoted as R.

The complete set of regeneration reactions that have been studied in this work is summarized in Figure 1. The three initial $Mn^{III}\cdots OX$ complexes ($Mn^{III}\cdots OR$ (**H**), $Mn^{III}\cdots OH$ (**L**), and $Mn^{III}\cdots OOR$ (**O**)) are highlighted with a solid-line square. As mentioned in previous works, the stable electronic configuration of these complexes is with the unpaired electrons contributed by Mn^{III} and $\cdot OX$ in opposite spins.[24] Regeneration could, in principle, take place from any of the $Mn^{III}\cdots OX$ complexes; however, $Mn^{III}\cdots OR$ (**H**) and $Mn^{III}\cdots OH$ (**L**) are transformed into $Mn^{III}\cdots OOR$ (**O**) through the propagation reactions, and so the latter represents the final product of the propagation pathway, and as such, it is the main species from which regeneration should take place.

A. Conversion of $Mn^{III}\cdots OOR$ into $Mn^{III}\cdots OH$ (O → L). Iglesia et al.[15] suggested that complex $Mn^{III}\cdots OOR$ (**O**) could be transformed into $Mn^{III}\cdots OH$ (**L**) by means of an intramolecular H-transfer from the methylene C atom in $\cdot OOR$ ($\cdot OO\mathbf{C}H_2CH_3$), prompting our interest in studying this transformation computationally. This reaction would provide a conversion between complexes $Mn^{III}\cdots OOR$ (**O**) and $Mn^{III}\cdots OH$ (**L**), and so, if energetically viable, it would imply that both **O** and **L** complexes rather than **O** alone could lead to regeneration of the Mn^{II} active sites.

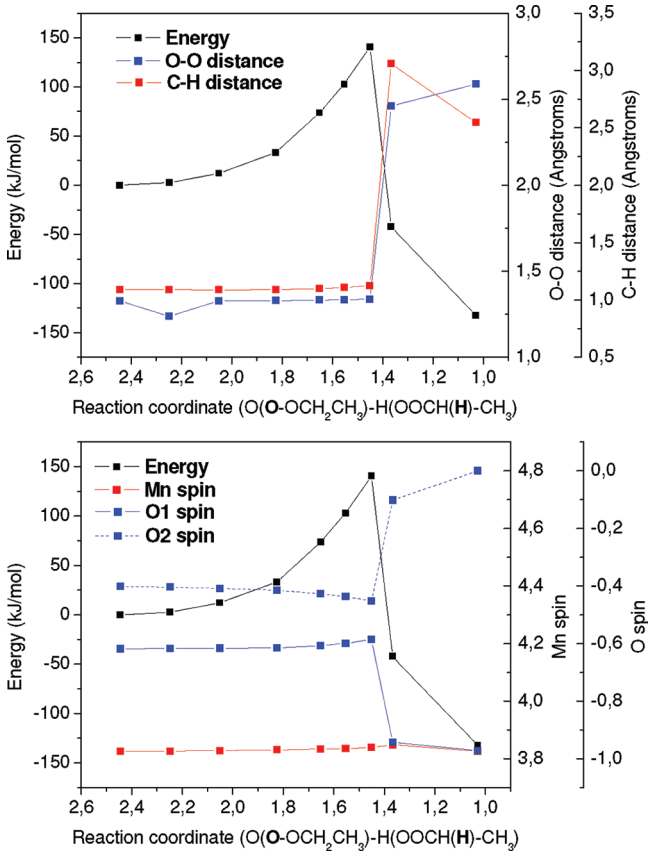

Figure 2. Top: Energy diagram (black line) and evolution of the O—O (blue line) and C—H (red line) distances along the reaction coordinate (represented as the distance between the H atom in methylene C and the terminal O atom in CH_3CH_2OO ($O(\mathbf{O}-OCH_2CH_3)-H(OO-C\mathbf{H}(H)CH_3)$ distance) for the intramolecular H transfer, which transforms $Mn^{III}\cdots OOR$ (**O**) into $Mn^{III}\cdots OH$ (**L**). Bottom: Energy diagram (black line) and evolution of the Mn (red line), O1 ($CH_3CH_2\mathbf{O}O$, solid blue line), and O2 ($CH_3CH_2O\mathbf{O}$, dashed blue line) spin densities along the reaction.

The energy profile for this reaction step is displayed in Figure 2; the molecular structures of the reactants (**O**), TS ($TS_{O\rightarrow L}$), and products (**L**) are shown in Figure 3; Figure 2 in the Supporting Information (Figure 2-SI) shows the corresponding spin density maps. The reaction coordinate was selected as the distance between the H atom to be transferred and the terminal O that uptakes it; the initial distance between these atoms was 2.445 Å (see Figure 3, top-right, dashed blue line). The energy diagram shows a very high activation energy of 141 kJ/mol, after which the energy decreases dramatically, giving a reaction enthalpy of −132 kJ/mol. These energy results indicate the formation of a stable product, but with a very unfavorable TS.

The structure of the latter is shown in Figure 3 (middle), where we observe that the transferring H atom is shared between the C atom and the terminal O, forming a 4-membered ring. At

dx.doi.org/10.1021/cs200402b |ACS Catal. 2011, 1, 1475–1486

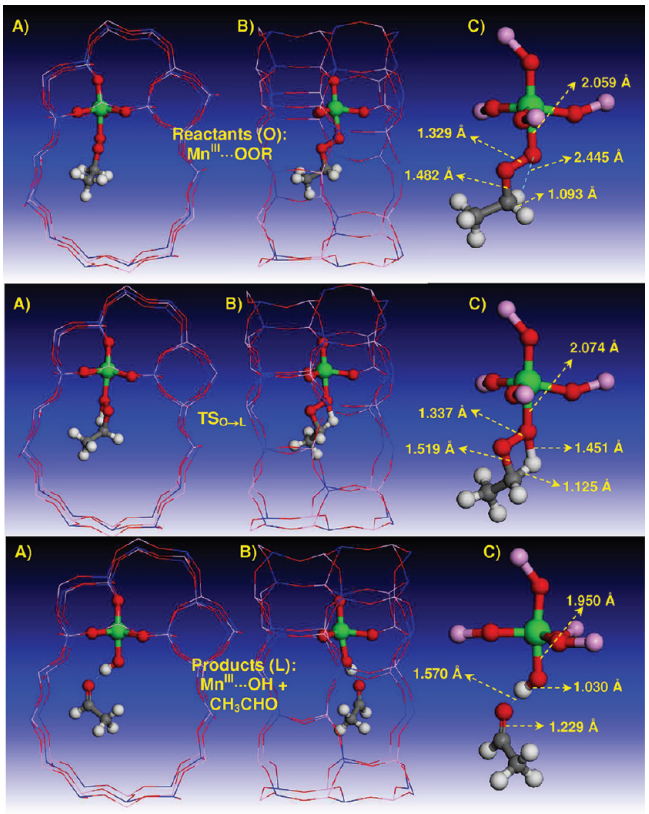

Figure 3. Two views (A and B) and detail (C) of the structure of the reactants (**O**) (top), transition state ($\mathbf{TS_{O\rightarrow L}}$) (middle) and products (**L**) (bottom) for the intramolecular H-transfer that transforms complex **O** into **L**, yielding a molecule of aldehyde (**O** → **L**).

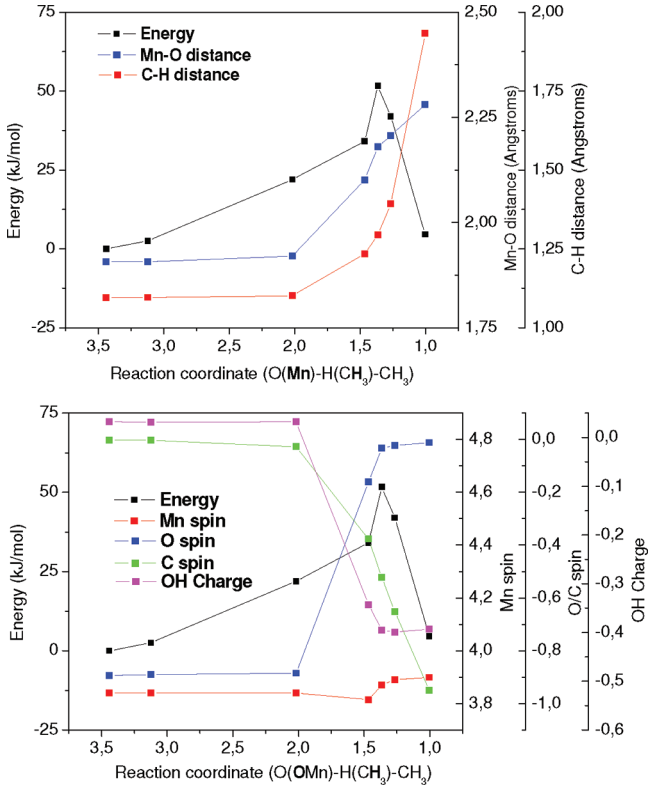

Figure 4. Top: Energy diagram (black line) and evolution of the O−Mn (blue line) and C−H distances (red line) along the reaction coordinate (represented as the distance between a H atom in CH_3CH_3 and the (nearest neighbor to Mn) framework O atom (O(Mn)−H(CH_3CH_3) distance) for the H transfer from ethane to the framework O atom (**L** → **R**) in $Mn^{III}\cdots OH$ (**L**). Bottom: Energy diagram (black line) and evolution of the C (green line), O (from the hydroxo OH ligand, blue line), and Mn (red line) spin densities and of the OH charge (pink line) along the reaction.

this point (TS), the spin distribution is very similar to that of the reactants, as shown by the spin-density evolution (Figure 2, bottom) and their respective spin-density maps (Figure 2-SI). Beyond the TS, a dramatic increase in the C−H distance is observed (red line in Figure 2, top), evidencing the dissociation of this bond. Such dissociation is accompanied by a dissociation of the O−O bond (blue line in Figure 2, top), leading to the formation of an OH ligand bonded to Mn. Indeed, the spin polarization of the hydroxyl O atom (O2, dashed blue line in Figure 2, bottom) decreases to −1, indicating the formation of a radical-type ligand (·OH), as also evident from the spin density maps of the products (Figure 2-SI, right). Instead, the nonterminal O (O1, solid blue line in Figure 2, bottom) is not spin-polarized, since the unpaired electrons originating in the homolytic cleavage of C−H and O−O bonds couple to form a C═O double bond, thus yielding an aldehyde molecule (Figure 3, bottom). The C═O double bond nature is confirmed by the decrease in the C−O distance from 1.482 to 1.229 Å. In this chemical transformation, Mn does not undergo any redox process (red line in Figure 2, bottom). The stability of the aldehyde molecule formed explains the exothermic nature of this step.

This mechanistic pathway provides a route for transforming the final product of the propagation cycle, $Mn^{III}\cdots OOR$ (**O**), into complex $Mn^{III}\cdots OH$ (**L**) and also accounts for the formation of the aldehyde, one of the known oxidation products, but does not enable itself a regeneration of the Mn sites, since Mn does not undergo any redox process. Since conversion of complex **O** into **L** is possible, two Mn species are available for regeneration: $Mn^{III}\cdots OOR$ (**O**) and $Mn^{III}\cdots OH$ (**L**).

B. Regeneration by H Transfer to Framework O. The active site required in the oxidation cycle for decomposition of the hydroperoxide molecules is Mn^{II} with an acid proton bonded to one of its four nearest neighbor O sites (**F**).[24] This can be obtained from Mn^{III} by uptake of a H atom by a framework O, whereas the electron associated with H is transferred to Mn resulting in its reduction. This is the same mechanism whereby initial preactivation of the calcined Mn^{III} sites takes place, with H being transferred from the hydrocarbon. Therefore, a possible mechanistic route to accomplish the catalyst regeneration from $Mn^{III}\cdots OOR$ (**O**) or $Mn^{III}\cdots OH$ (**L**) involves a H transfer from hydrocarbon molecules not to the radical O atom of the ·OOR or ·OH ligands (which would lead to a propagation cycle[25]), but to the framework O nearest neighbor to Mn. Propagation and regeneration reactions are therefore competitive. For completeness, the corresponding H transfer to complex $Mn^{III}\cdots OR$ (**H**) was also studied. The H abstraction examined here leads to R· radicals that will then couple to the O-based ligand (OH, OR, or OOR), to form a closed-shell O-containing species (ROH, ROR, or ROOR, respectively), which after desorption from Mn will yield a free Mn^{II} site (**F**), thus achieving the required regeneration of the Mn active sites. Let us examine

dx.doi.org/10.1021/cs200402b |ACS Catal. 2011, 1, 1475–1486

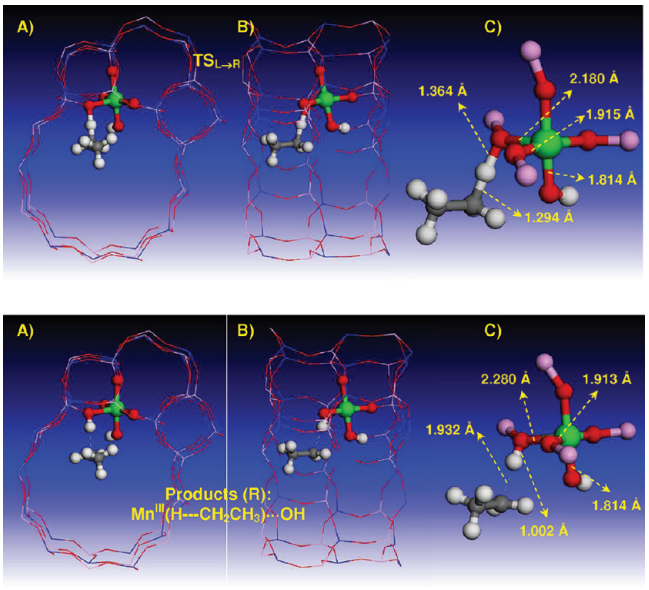

Figure 5. Two views (A and B) and detail (C) of the structure of the transition state ($\mathbf{TS_{L\rightarrow R}}$) (top) and of the products (**R**) (bottom) for the H transfer from ethane to the framework O nearest neighbor to Mn^{III} (**L** → **R**) in Mn^{III}···OH (**L**).

the mechanistic details of this reaction, from the three possible complexes (**L**, **H**, and **O**).

*B.1. Mn^{III}···OH (**L** → **R** → **S** → **F**).* We discuss in detail the mechanistic route for the Mn^{III}···OH (**L**) complex and then extend the results to the other complexes (**H** and **O**). The energy diagram for the H-transfer reaction from ethane to the framework O nearest neighbor to Mn is shown in Figure 4. The reaction coordinate for this elementary step was selected as the distance between the H atom of the hydrocarbon that is being transferred and the framework O atom that uptakes it. As observed in ref 24, of the four framework O atoms nearest neighbor to Mn, the most stable location for the proton corresponds to the one that is part of a 4- and a 12-membered ring; therefore, this was selected as the framework O to which the H is transferred. The energy diagram shows an activation energy of 52 kJ/mol and a slightly endothermic enthalpy of +4 kJ/mol. As expected, this H transfer prompts the dissociation of the C−H bond in the hydrocarbon, as evidenced by the increase in the C−H distance along the reaction coordinate (Figure 4-top, red line).

In addition, we observe an increase in the distance between Mn and the framework O atom to which the H is transferred (Figure 4, top, blue line). The evolution of the atomic spin polarization for the different species involved in this reaction (Figure 4, bottom) shows that the spin of the C atom from which the H is transferred varies from 0 (in the hydrocarbon) to −1, consistent with the formation of an ethyl radical R· via a homolytic C−H bond dissociation. Unexpectedly, we observe that the Mn spin does not vary: it remains ∼3.8 all along the reaction coordinate, corresponding to Mn in the 3+ oxidation state. However, we would expect a reduction of Mn with the H transfer, since the electron coming from H should be transferred to Mn to give Mn^{II}, as occurred in the preactivation step on the bare Mn^{III} sites. Instead, we observe that the O atom from the hydroxo ligand, which initially is spin-polarized, since the OH ligand has a radical nature, changes its spin from −1 to 0, leading to a closed-shell hydroxide anion. This result is unexpected, since in principle, this hydroxo ligand does not intervene directly in the H transfer; however, our results show that the hydroxo ligand is a better electron acceptor than Mn^{III} in this reaction environment. The charge of the OH species along the reaction (Figure 4, bottom, pink line), shows a steady decrease at reaction coordinates below 2.0 Å, showing that OH indeed becomes anionic and confirming the uptake of the electron by OH rather than by Mn.

Figure 5 shows the molecular structure of the TS ($\mathbf{TS_{L\rightarrow R}}$) (top) and products (**R**) (bottom) for this reaction: the H transfer and the consequent formation of an ethyl radical R· can be clearly appreciated. As in all the H transfers from RH discussed in the catalytic cycle, the resulting R· radical is not free inside the channel but remains linked to the framework by a strong interaction between the radical C atom and the transferred H atom now bonded to the framework. Instead, the R· radical does not interact with the OH ligand. As expected, the Mn−O distance with the framework O that takes up the H atom increases (by ∼0.1 Å) with respect to the others due to the formation of an additional bond in the O atom. This is a common feature of OH groups in zeolites and AlPOs.

Figure 6 shows the spin-density maps for the reactants (**L**), TS ($\mathbf{TS_{L\rightarrow R}}$) and products (**R**) of this elementary step. In the reactants, the α spin density (displayed in red) is localized mainly on the Mn atom, and the β spin density (displayed in blue) is localized on the O atom of the HO· ligand, confirming its radical nature. In the TS and especially in the products, the β spin density is localized mainly on the C atom of the hydrocarbon (which becomes a radical), confirming the homolytic dissociation of the C−H bond. Instead, the β spin density on the HO· ligand vanishes due to its transformation into a hydroxide anion.

At this point (**R**), we have the ethyl radical R· and an anionic OH^- ligand forming a complex with Mn^{III}. Despite the H atom's having been transferred to the framework O, Mn is still in the oxidized state, since the electron has been transferred to the ligand and not to the metal. A further step is required to regenerate the Mn^{II} sites. The ethyl radical R· formed is very reactive; in the presence of O_2, it forms a free peroxo radical, as in the propagation reactions. This would yield the active site with an anionic hydroxide and a proton (H^+) attached, which would rapidly recombine to form water, a free Mn^{III} site, and a free peroxo radical; that is, intermediate **K** in the propagation reactions.[25]

Alternatively, the R· radical in **R** can approach the OH ligand to form a new O−C bond and yield an ethanol molecule (**S**). The energy diagram for this reaction is shown in Figure 7. In this case, the reaction coordinate corresponds to the distance between the atoms involved in the new bond to be formed: the radical C atom in R· and the O atom in the OH ligand. A negligible activation energy is required for this process (∼10 kJ/mol), and indeed, this is an extremely exothermic reaction (−244 kJ/mol), since it forms a very stable species, the ethanol molecule (**S**) (Supporting Information Figure 3, left). The formation of this new C−O bond involves the disconnection between the ethyl radical and the proton attached to the framework, as evidenced by the increase in the distance between the radical C and the framework proton (Figure 7, top, red line), which causes the small activation energy of this reaction step. The transformation of the hydroxide ligand into ethanol causes an increase in the bond distance between Mn and the O-based ligand (blue line).

The evolution of the spin polarization (Figure 7, bottom) clearly indicates that Mn is finally reduced in this step: its spin increases to 4.8, corresponding to Mn^{II} (red line); coupling with

dx.doi.org/10.1021/cs200402b |*ACS Catal.* 2011, 1, 1475–1486

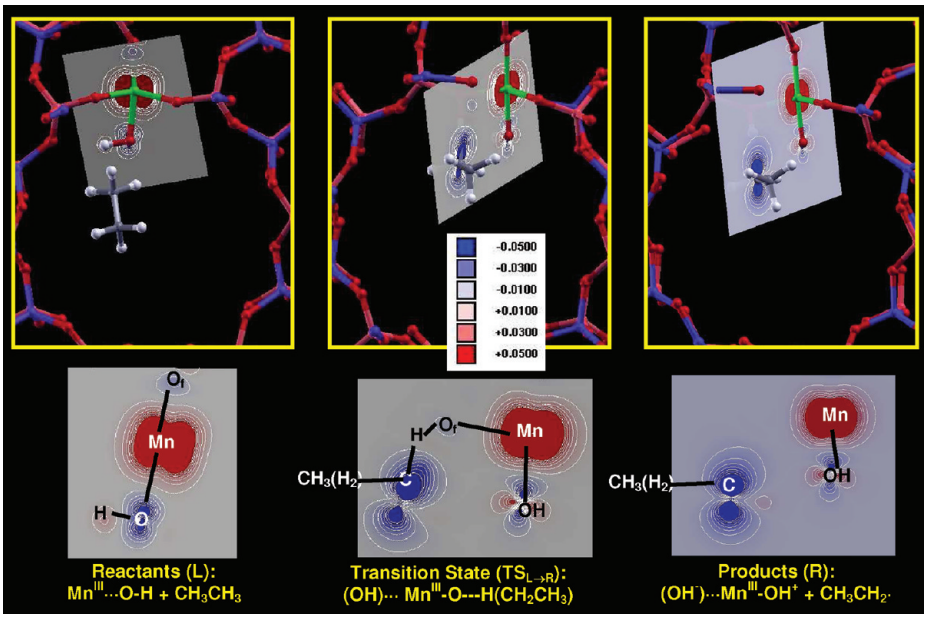

Figure 6. Spin-density maps of the reactants (**L**) (left), transition state ($\mathbf{TS_{L\rightarrow R}}$) (middle), and products (**R**) (right) for the H transfer from ethane to the framework O atom (**L** → **R**) in $Mn^{III}\cdots OH$ (**L**); β and α spin densities are displayed in blue and red, respectively. White lines indicate isodensity lines. For the sake of clarity, the same maps are displayed at the bottom without the atoms.

the R· radical to form ethanol requires an OH radical rather than the OH^- originally formed. The electron previously taken by the OH ligand is transferred back to Mn so that the resulting radical OH species forms a bond with the radical C atom, with each species providing one electron to form the new C−O bond in the ethanol product. The spin polarization of C and O also disappears upon this process (green and blue lines, respectively, in Figure 7, bottom). The reduction of Mn to the stable 2+ oxidation state and the formation of a stable ethanol molecule are responsible for the highly exothermic nature of this step (−244 kJ/mol).

A final desorption of ethanol, a process with a slightly endothermic enthalpy of +19 kJ/mol, frees the Mn^{II} active site so that it can adsorb new hydroperoxide molecules, thus providing a regeneration route.

*B.2. $Mn^{III}\cdots OR$ (**H** → **BF** → **BG** → **F**).* Let us now consider the reaction steps equivalent to those discussed in section B.1, but starting from complex $Mn^{III}\cdots OR$ (**H**), which lead to the formation of a diethyl ether molecule (ROR). The energy diagram for the initial H transfer to the framework (**H** → **BF**) (Supporting Information Figure 4) shows an activation energy for this process of 101 kJ/mol and an endothermic reaction enthalpy of 60 kJ/mol. Atomic (Supporting Information Figure 5) and spin (Supporting Information Figure 6) rearrangements similar to those discussed in section B.1 are observed in this case, indicating that a similar chemical reaction takes place: a homolytic dissociation of the C−H bond in RH, giving place to an ethyl radical R· and a H transfer to the framework O, with a consequent transfer of the electron from H not to Mn^{III}, but to the RO· ligand, yielding an ethoxide anion (RO^-) (**BF**), as evidenced by the spin-polarization evolution (Figures 4-SI, right and 6-SI). The C spin in **BF** is −1 and the O spin is 0 (green and blue lines in Figure 4-SI, right, respectively). Mn remains as Mn^{III} (red line); it is reduced in a subsequent step by taking up the electron from the ethoxide anion, which becomes a radical upon coupling with the radical R· to form a diethyl ether molecule, ROR (**BG**) (Figure 3-SI, middle). This process is very exothermic (−246 kJ/mol) and promotes the transfer of the electron from the ethoxide anion to Mn, as shown by the Mn spin in **BG** of 4.82 (d^5, Mn^{II}). A final desorption of ROR (ΔH = +11 kJ/mol) yields the free Mn^{II} site.

*B.3. $Mn^{III}\cdots OOR$ (**O** → **BC** → **BD** → **F**).* The same set of reactions can occur for complex **O** ($Mn^{III}\cdots OOR$). The calculated reaction profile for the initial H transfer from ethane to the framework O (Supporting Information Figure 7) shows an activation energy of 162 kJ/mol and an endothermic reaction enthalpy (+129 kJ/mol); these values are much higher than those observed earlier from complexes **L** (E_a = 52 kJ/mol) and **H** (E_a = 101 kJ/mol), suggesting that this is a very unfavorable process for complex **O**. Atomic (Supporting Information Figure 8) and spin (Supporting Information Figure 9) rearrangements similar to those in sections B.1 and B.2 were observed, confirming that the homolytic C−H bond dissociation to produce R· radicals occurs in the same way: H is transferred to the framework O, and its electron is donated to the peroxo radical to form a peroxide anion ROO^- (**BC**) (Figure 7-SI, right, blue lines). Mn remains in an oxidation state of 3+ (red line); however, in this case, the Mn spin population slightly increases (from 3.83 to 4.03), suggesting a lower ability of ROO to form an anionic species. A subsequent coupling of the R· radical to the peroxide anion prompts a transfer of the peroxide electron to Mn, causing its reduction, as evidenced by its spin of 4.82 (d^5, Mn^{II}), and allowing the formation of a new C−O bond between the unpaired electrons of R· and ROO·, respectively, yielding a molecule of diethyl peroxide (ROOR) (Figure 3-SI, right), which forms a complex with reduced Mn^{II} (**BD**). As in previous cases, this process is very exothermic (−250 kJ/mol) due to the formation of a C−O bond and the Mn reduction. ROOR is finally desorbed from Mn (ΔH = +2 kJ/mol) to yield free Mn^{II} sites, thus achieving the Mn regeneration.

C. Regeneration by H Transfer from Ethanol (O → T → BE → F). As discussed earlier, complex $Mn^{III}\cdots OOR$ (**O**)

dx.doi.org/10.1021/cs200402b |*ACS Catal.* 2011, 1, 1475–1486

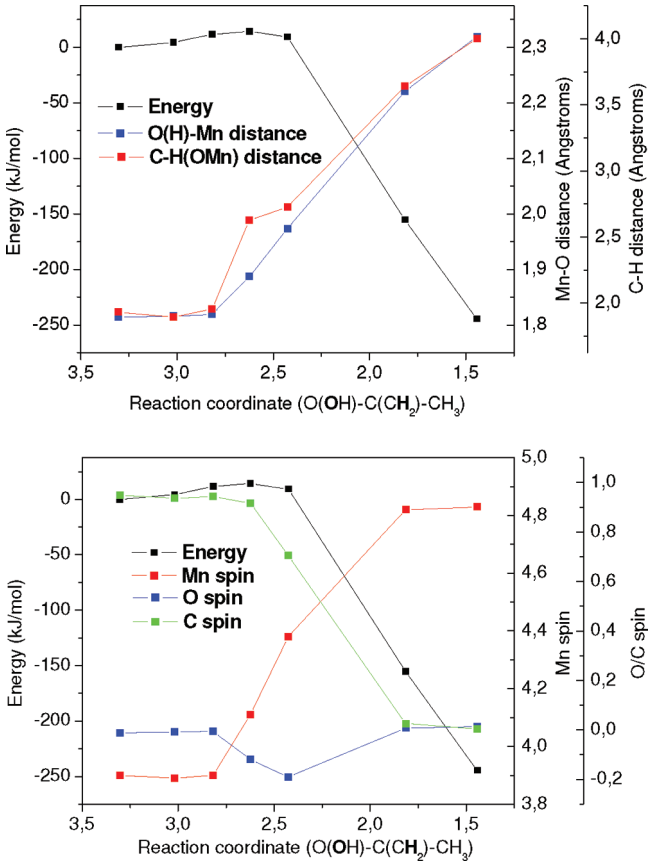

Figure 7. Top: Energy diagram (black line) and evolution of the framework O (from ligand)−Mn (blue line) and C−H (H bonded to OMn) distances (red line) along the reaction coordinate (represented as the distance between the radical C atom in CH_3CH_2 and the O atom of the OH ligand (O(OH)−C(CH_2CH_3) distance) for the coupling between CH_3CH_2 and OH to form CH_3CH_2OH (**R** → **S**). Bottom: Energy diagram (black line) and evolution of the C (green line), O (from the hydroxo OH ligand, blue line), and Mn (red line) spin densities.

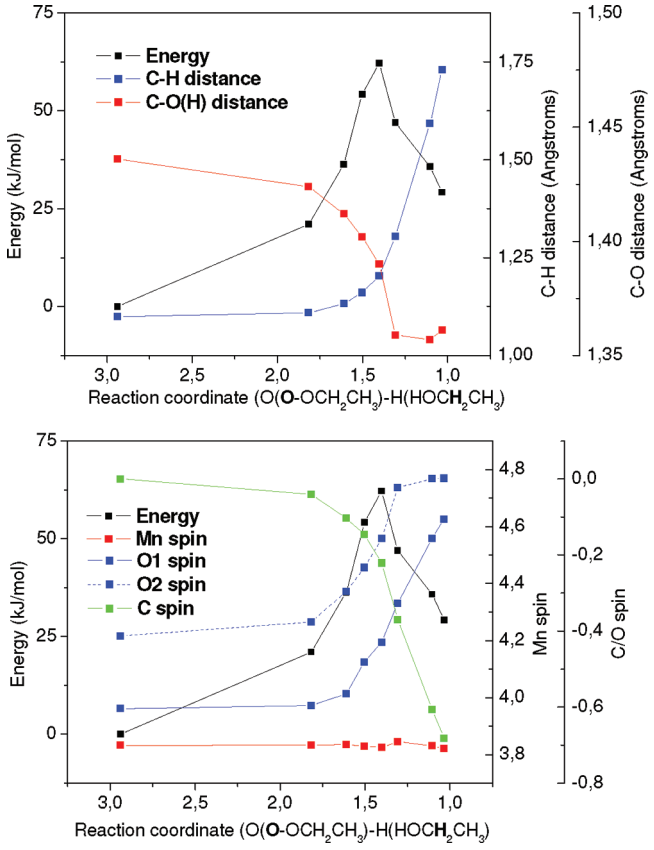

Figure 8. Top: Energy diagram (black line) and evolution of the C−H (blue line) and C−O(H) (hydroxy group) distances (red line) along the reaction coordinate (represented as the distance between the H atom bonded to methylene C in CH_3CH_2OH and terminal O atom in CH_3CH_2OO (O(O−OCH_2CH_3)−H(HO−CH_2CH_3) distance) for the H transfer from ethanol to $CH_3CH_2OO\cdot$ (**O** → **T**) in $Mn^{III}\cdots OOCH_2CH_3$ (**O**). Bottom: Energy diagram (black line) and evolution of the C (green line), O (from the peroxo OOR ligand (terminal O, solid blue line; nonterminal O, dashed blue line), and Mn (red line) spin densities.

represents the main species from which regeneration should take place, since propagation reactions from all the $Mn^{III}\cdots OX$ complexes terminate with the production of intermediate **O**. Despite the existence of the mechanistic pathway to transform **O** into $Mn^{III}\cdots OH$ (**L**) discussed in section A, its high activation energy of 141 kJ/mol implies that the main Mn species from which Mn is to be regenerated is still $Mn^{III}\cdots OOR$ (**O**). The pathway discussed in section B, while likely on energetic grounds from intermediate **L**, is not a plausible regeneration mechanism from intermediate **O**, since it involves a very high activation energy (162 kJ/mol) and a very endothermic reaction enthalpy (+129 kJ/mol). Indeed, the competitive mechanism in which a H transfer takes place not to the framework O but to the radical O atom in ROO·, which leads to the propagation subcycle from $Mn^{III}\cdots OOR$ (**O**),[25] with E_a = 84 kJ/mol and ΔH = +78 kJ/mol, is expected to be the predominant evolution path from intermediate **O**. Therefore, it becomes clear that there must be an alternative regeneration mechanism from complex **O**.

It appears that no other chemical transformations involving the initial reactants, that is, the hydrocarbon and O_2, other than those already shown are available for the reduction of Mn in $Mn^{III}\cdots OOR$ (**O**). However, at this point of the reaction, new species resulting from the initial oxidations start to accumulate in the catalyst pores; namely, ROH and H_2O (from ROOH decomposition[24] and propagation[25] reactions). H_2O is inert under these conditions; in contrast, the alcohol ROH is an active species that could participate in the regeneration of the Mn active sites and transform itself into new oxidation products.

Let us consider therefore the reaction pathway for the regeneration of the Mn active sites in $Mn^{III}\cdots OOR$ (**O**) in the presence of ethanol (ROH). Reduction of Mn^{III} requires a radical H abstraction from the organic substrate ROH. There are three types of H atoms in ethanol (CH_3CH_2OH): the H bonded to O, to C_α, or to C_β, whose calculated bond energies are 442, 417, and 462 kJ/mol, respectively. The most readily available H atom is the one bonded to C_α. Indeed, its C−H bond energy (417 kJ/mol) is much lower than that of the RH hydrocarbon (454 kJ/mol), showing the more active character of ROH compared with RH. The more active nature of this H atom enables its transfer to the terminal O atom of the ROO· ligand in $Mn^{III}\cdots OOR$ (**O**) to yield an ROOH molecule bonded to Mn^{III} and the corresponding hydroxy-containing radical $CH_3CH\cdot(OH)$ (**T**).

The energy diagram for this step (**O** → **T**) is shown in Figure 8, where the reaction coordinate was selected as the distance between the H being transferred and the terminal O in ROO. The energy profile shows an activation energy of

dx.doi.org/10.1021/cs200402b |*ACS Catal.* 2011, 1, 1475–1486

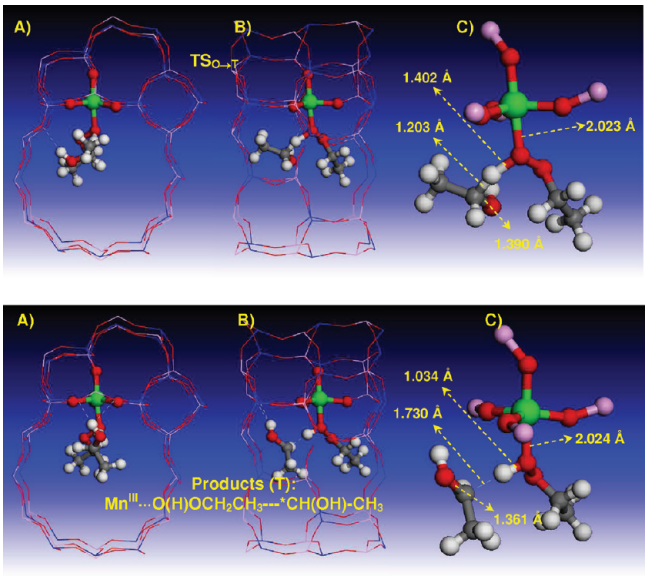

Figure 9. Two views (A and B) and detail (C) of the structure of the transition state ($\mathbf{TS_{O\rightarrow T}}$) (top) and of the products (**T**) (bottom) for the H transfer from ethanol to $CH_3CH_2OO\cdot$ (**O** → **T**) in $Mn^{III}\cdots OOCH_2CH_3$ (**O**).

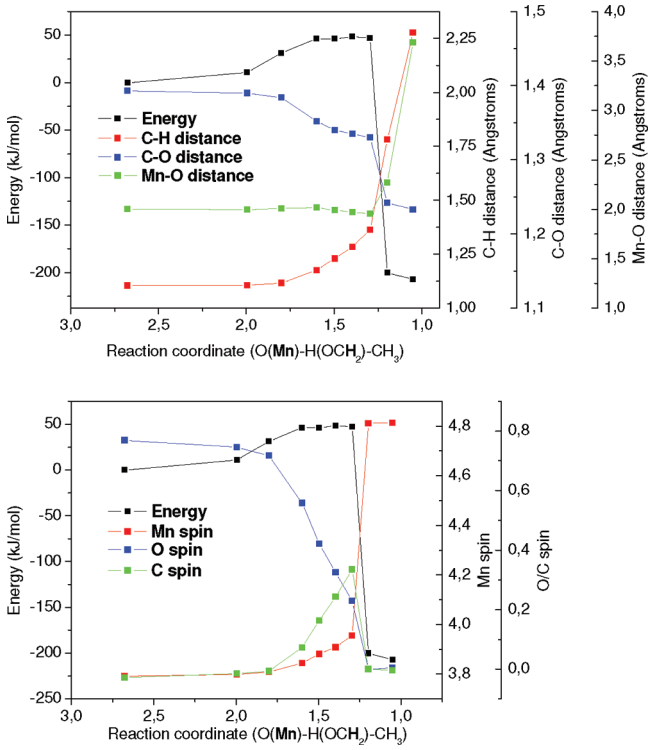

Figure 10. Top: Energy diagram (black line) and evolution of the C−H (red line), C−O (blue line), and Mn−O (green line) distances along the reaction coordinate (represented as the distance between the H atom bonded to the methylene C in $CH_3CH_2O\cdot$ and the framework O atom (O(Mn)−H(OCH_2CH_3) distance) for the unimolecular H transfer from $Mn^{III}\cdots OCH_2CH_3$ (**H** → **BE**). Bottom: Energy diagram (black line) and evolution of the C (green line), O (from the ·OR ligand), and Mn (red line) spin densities.

62 kJ/mol and a reaction enthalpy of +29 kJ/mol. These energies are lower than the corresponding ones for the H transfer from the hydrocarbon (E_a = 84 kJ/mol; ΔH = +78 kJ/mol; step **O** → **P**), confirming the higher reactivity of ROH. The approach of the H atom to the radical O atom in ROO· involves a progressive homolytic dissociation of the corresponding C−H bond (Figure 8, top, blue line), leading to the formation of an ethyl radical, as showed by the change of the C spin from 0 to −0.7 (Figure 8, bottom, green line). The final C spin in the 1-hydroxyethyl $CH_3CH\cdot(OH)$ radical is not −1, due to a partial delocalization of the spin density to the hydroxy group.

The formation of the 1-hydroxyethyl radical causes a rehybridization to sp^2 of the radical C, accompanied by a shortening of the C−O bond with the hydroxy group from 1.44 to 1.36 Å (Figure 8, top, red line). The unpaired electron is therefore occupying a C−O unit with partial double bond character. The electron transferred with the H atom is used to form a new O−H bond with the terminal O atom in ROO·, as shown by the decrease in the spin polarization on the two O atoms to ∼0 (Figure 8, bottom, blue lines). No redox process takes place on the Mn site (red line); it remains as Mn^{III}, ruling out the transfer of an electron to or from Mn during this step.

The structure of the TS ($\mathbf{TS_{O\rightarrow T}}$) and products (**T**) is shown in Figure 9 (top and bottom, respectively), where the transfer of the H atom from ROH to ROO· is clear. The radical C atom in $CH_3CH\cdot(OH)$ is in a nearly planar environment, typical of sp^2 hybridization with the unpaired electron located in the p atomic orbital perpendicular to the plane. As in previous cases, the stereochemistry of this H transfer leaves a strong interaction between the nascent radical and the H atom transferred to ROO, as observed in Figure 9 (bottom, dashed blue line). The spin density maps of reactants (**O**), TS ($\mathbf{TS_{O\rightarrow T}}$), and products (**T**) (Figure 10-Supporting Information) confirm the electronic rearrangement of this mechanism, and so the homolytic nature of the C−H bond dissociation and H transfer. The β spin density (blue) is progressively transferred from the ROO· radical to the C atom, whose C−H bond is dissociated, although some spin polarization (∼0.1) still remains on the terminal O atom in ROOH. Instead, the Mn spin density (red) is not modifed throughout the process. The spin density of the radical C atom is asymmetrically oriented toward the transferred H atom due to the interaction between the two.

At this point, Mn is still in the oxidized state (III), and so it needs to be reduced to regenerate the active sites. To do so, a H atom has to be transferred to a framework O atom nearest neighbor to Mn in such a way that the electron transferred with the H atom is taken up by Mn, yielding a regenerated Mn^{II} active site (**F**) with the attached proton. The most weakly bonded H atom in radical $CH_3CH\cdot(\mathbf{OH})$ is that in the hydroxy group (highlighted in bold), with an O−H bond energy of 138 kJ/mol. This bond is so weak (XH bond energies are usually in the 400−500 kJ/mol range) since the oxygen is engaged in a partially double bond with C to delocalize the unpaired electron. Homolytic dissociation of the OH bond yields a very stable molecule, the aldehyde ($CH_3CH\cdot(O-\mathbf{H}) \rightarrow CH_3CH(=O) + \mathbf{H}\cdot$). In the catalyst, the resulting H atom would be stabilized by binding to the framework O and transferring the electron to Mn. Therefore, it is reasonable to expect the hydroxy H atom to be easily transferable to the framework O to regenerate the Mn active sites (**F**) (**T** → **BE**).

To examine this step, the H−O distance was selected as the reaction coordinate representative of this elementary step. Our results indicate that OH cleavage requires no activation energy

dx.doi.org/10.1021/cs200402b |ACS Catal. 2011, 1, 1475–1486

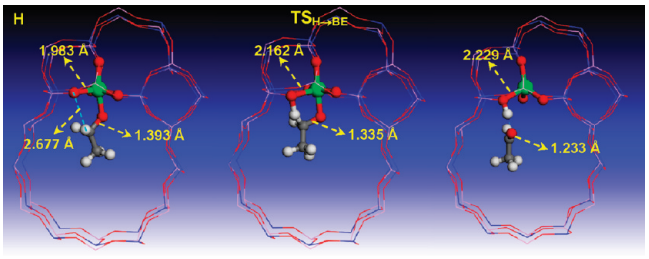

Figure 11. Molecular structure of reactants (**H**) (left), **TS** (middle) and product (**BE**) of the unimolecular H transfer from $Mn^{III}\cdots OCH_2CH_3$ (**H** → **BE**).

and has a very exothermic enthalpy (−168 kJ/mol), which is explained by the formation of two stable species: the aldehyde and a Mn^{II} site, with Mn in the most stable oxidation state (Supporting Information Figure 11) (**BE**). The homolytic dissociation of the O−H bond generates an ethanal molecule with a double C═O bond, as shown by the decrease in the C−O distance from 1.361 to 1.235 Å (Figure 11-SI). This step also requires desorption of the ROOH molecule from Mn due to the steric hyndrance caused by the $CH_3CH\cdot(OH)$ radical approaching the framework O (**BE**) (Figure 11-SI). In the resulting products, the framework proton is bent toward the 12-membered ring channel due to the development of a H bond interaction with the basic O atom of the aldehyde. Such H bond interaction is strong, as shown by the short O···H distance of 1.464 Å (Figure 11-SI). The final Mn spin-density of 4.82 shows its reduction in this step (Figure 11-SI, right). Finally, to recover the free Mn^{II} sites able to reinitiate the oxidation cycle (**F**), the aldehyde molecule needs to be desorbed from the framework proton, a process that requires a desorption energy of 38 kJ/mol, confirming the strong H bond interaction between these species. After desorption of the aldehyde, the framework proton locates in its most stable orientation, within a 6-membered ring of the framework wall.

In summary, the pathway (**O** → **T** → **BE** → **F**) discussed here provides a mechanistic route for the regeneration of the Mn^{II} sites from complex $Mn^{III}\cdots OOR$ (**O**), producing a secondary oxidation of the ethanol molecule into an aldehyde. Similar secondary oxidations can take place from $Mn^{III}\cdots OR$ (**H**) and $Mn^{III}\cdots OH$ (**L**) complexes, and will be discussed in a forthcoming paper, dedicated to a complete analysis of the possible secondary oxidation routes leading to the formation of aldehyde and acid, both experimentally observed reaction products.

D. Unimolecular H Transfer from $Mn^{III}\cdots OR$ (H) to Framework O (H → BE). We envisaged another mechanism for the regeneration of the Mn sites, in this case, from complex $Mn^{III}\cdots OR$ (**H**). This is not the final product of the oxidation cycle, since this intermediate evolves to form complex $Mn^{III}\cdots OOR$ (**O**), and so this pathway does not represent a main regeneration route. For completeness, however, we include this mechanistic path in the current discussion (Figure 10). In complex $Mn^{III}\cdots OR$ (**H**), a H atom of the methylene C is located close to the framework O atom nearest neighbor to Mn, at a distance of 2.677 Å (see Figure 11, left). This proximity may eventually enable a unimolecular H transfer from this C to the framework O, leading to the regeneration of the Mn active sites. We selected the aforementioned H−O distance as the reaction coordinate to study this pathway.

The energy diagram is shown in Figure 10, and the molecular structure of the species involved is displayed in Figure 11. This

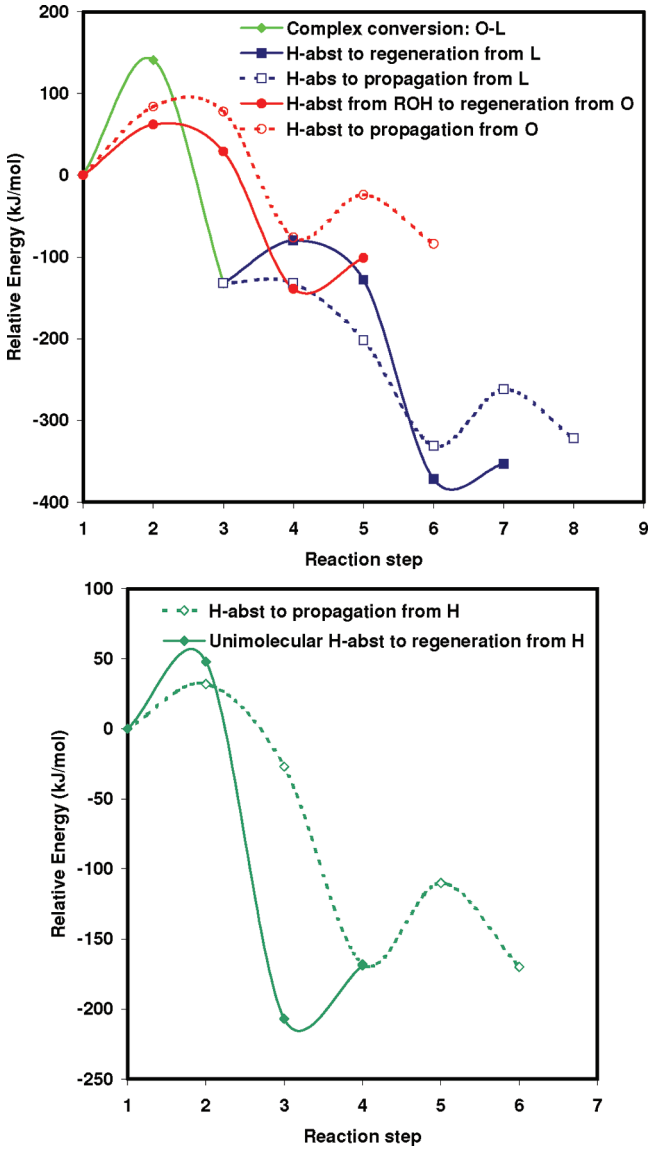

Figure 12. Summary of the energetic results for the regeneration and competitive propagation mechanisms from complex $Mn^{III}\cdots OOR$ (**O**) and $Mn^{III}\cdots OH$ (**L**) (top) and from $Mn^{III}\cdots OR$ (**H**) (bottom). (Top) Green line: conversion of complex **O** into **L**, with formation of an aldehyde molecule (**O** → **L**). Solid blue line: regeneration from **L** by H transfer from ethane to framework O and subsequent ROH formation (**L** → **R** → **S** → **F**). Dashed blue line: propagation from **L** by H transfer from ethane to OH and subsequent O_2 addition, H_2O desorption, and ROO· binding (**L** → **M** → **N** → **K** → **O**). Solid red line: regeneration from **O** by H transfer from ROH to ROO·, subsequent H-transfer to framework, and final desorption of the produced aldehyde (**O** → **T** → **BE** → **F**). Dashed red line: propagation from **O** by H transfer from ethane to ·OOR and subsequent O_2 addition, ROOH desorption, and ROO· binding (**O** → **P** → **Q** → **K** → **O**). (Bottom) Solid line: regeneration mechanism from H by unimolecular H transfer from RO ligand to framework and subsequent desorption of aldehyde (**H** → **BE** → **F**). Dashed line: propagation from **H** by H transfer from ethane to RO and subsequent O_2 addition, ROH desorption, and ROO· binding (**H** → **I** → **J** → **K** → **O**).

process has an activation energy of 48 kJ/mol and a very exothermic reaction enthalpy (−207 kJ/mol). The C−H bond is progressively dissociated (Figure 10, top, blue line) upon the H

dx.doi.org/10.1021/cs200402b |ACS Catal. 2011, 1, 1475–1486

Table 1. Summary of the Energies (in kJ/mol) of the Alternative H Transfers from Ethane (RH) to a Framework O, Leading to Regeneration of the Active Sites, or to Radical O Atom in OX Ligands, Leading to the Propagation Reactions and Preventing Regeneration; and H Transfer from Ethanol (ROH) to ROO in Complex O, Leading to Regeneration of Mn Active Sites

	H abstraction from ethane (RH)				H abstraction from ethanol (ROH)	
complex	ΔH H-abstract to framew O	E_a H-abstract to framew O	ΔH H abstract to OX	E_a H abstract to OX	ΔH H abstract to OOR	E_a H abstract to OOR
Mn^{III} (**A**)	+93	135				
$Mn^{III}\cdots OH$ (**L**)	+4	52	−70	No		
$Mn^{III}\cdots OR$ (**H**)	+60	101	−27	32		
$Mn^{III}\cdots OOR$ (**O**)	+129	162	+78	84	+29	62

atom approaching the framework O, which is accompanied by a decrease in the C−O distance (red line; from 1.393 to 1.233 Å; Figure 11), showing again the formation of a double bond (**BE**). The structure of the TS ($\mathbf{TS_{H\rightarrow BE}}$) (Figure 11, middle) shows the formation of a 5-membered ring, comprising the atoms involved in the H transfer and Mn. The increase in the Mn−O distance after the TS (Figure 10, top, green line) shows that this process involves the desorption of RO from Mn, as is also apparent from the structure of products **BE** (Figure 11, right).

The electronic rearrangement that takes place is displayed in Figure 10, bottom. This unimolecular H transfer involves a reduction of Mn, as shown by the increase in the Mn spin to ∼5 (red line) due to the transfer of the electron from the H atom. Simultaneously, the spin polarization of the initially radical O atom (blue line) disappears along the reaction; the unpaired electron located in the O atom is used for the formation of a double bond with the unpaired electron in the C atom arising from the homolytic C−H bond dissociation. Indeed, the C atom becomes spin-polarized in the transition state (green line), but its spin polarization disappears once the activation barrier is passed. Desorption of the aldehyde from the proton frees the Mn^{II} site, thus providing a new regeneration route. This alternative mechanism would close a new subcycle (**F** → **H** → **BE** → **F**), in which a hydroperoxide molecule is transformed into an aldehyde molecule and water ($CH_3CH_2OOH \rightarrow CH_3CH(=O) + H_2O$).

DISCUSSION

The aerobic oxidation of hydrocarbons in MnAPO-5 examined here has a complex reaction mechanism, that we have decomposed in the subsequent stages of preactivation, ROOH decomposition, propagation, and regeneration. Alternative propagation pathways exist, as discussed by us in an earlier work,[25] all of which terminate with the production of intermediate **O**, a complex between Mn^{III} and a peroxo radical ROO·. It is reasonable, therefore, to consider intermediate **O** as the main species from which regeneration of the Mn active sites must take place. In the regeneration reaction, the oxidized Mn^{III} active sites must be reduced to Mn^{II}, from which new oxidation cycles can take place.

In this work, we have identified computationally several mechanistic routes for this regeneration of the Mn active sites. The energy profile of the elementary steps for each regeneration mechanism is summarized in Figure 12. In general, regeneration of the 2+ oxidation state occurs via the homolytic cleavage of a C−H bond from an organic substrate, either the starting hydrocarbon CH_3CH_2−H or an alcohol $CH_3CH(OH)$−H. Uptake of radical H atoms takes place by leaving a proton (H^+) attached to a framework nearest neighbor to Mn while the electron is taken up by Mn^{III} that is thus reduced to Mn^{II}. The product is a $Mn^{II}(OH)$ active site, labeled as intermediate **F** in the overall reaction cycle, which represents the Mn active site for the initiation of the propagation cycle.

Propagation reactions lead to the formation of intermediate **O**, which must evolve into regenerated Mn^{II} sites for the reaction cycle to proceed. Other than to Mn^{II}, complex **O** can be transformed into $Mn^{III}\cdots OH$ (**L**) via the mechanism discussed in section A. This route has a very high activation barrier of 141 kJ/mol, but it is thermodynamically favorable as a result of its highly exothermic enthalpy (−132 kJ/mol). Thus, regeneration should take place mainly from $Mn^{III}\cdots OOR$ (**O**), but also to a certain extent from $Mn^{III}\cdots OH$ (**L**). The most obvious mechanism to achieve regeneration involves a H-transfer from a hydrocarbon molecule to a framework O atom nearest neighbor to Mn in $Mn^{III}\cdots OX$ complexes (**O** and **L**). In both cases, this H transfer is unfavored compared with the corresponding H transfer to the radical O atom in the oxo-containing ligand (OX) to form ROOH or H_2O, respectively (Table 1 and Figure 1). Such a regeneration pathway is energetically prohibitive for complex $Mn^{III}\cdots OOR$ (**O**), since it has a particularly high activation barrier (162 kJ/mol). Instead, this route is not so unfavorable for complex $Mn^{III}\cdots OH$ (**L**), for which the activation barrier is much lower (52 kJ/mol) (Figure 12, top, solid blue line). Nevertheless, the competitive H transfer to the OH ligand (no activation barrier; ΔH = −70 kJ/mol) and the following O_2 addition (ΔH = −129 kJ/mol) appear to be kinetically favored (Figure 12, top, dashed blue line). However, we should note that the subsequent step in the H transfer to the framework to complete the regeneration process (**R** → **S**) is extremely exothermic (−244 kJ/mol). In summary, the regeneration pathway (**L** → **R** → **S**) could take place under certain conditions, especially in the absence of alternative regeneration mechanisms, but will be slow for kinetic reasons.

It is interesting to note the low activation barriers for the H abstraction from ethane to the framework O of complexes $Mn^{III}\cdots OH$ (**L**) and $Mn^{III}\cdots OR$ (**H**) (52 and 101 kJ/mol, respectively), compared with the corresponding one for the same H abstraction from a bare Mn^{III} site (135 kJ/mol,[23] Table 1). These energies show that the radical ligands ·OH and ·OR in complexes **H** and **L**, respectively, increase the activity of the framework O atoms (nearest neighbor to Mn) for the homolytic cleavage of C−H bonds. The higher activity can be explained by the electron transfer not to Mn but to the radical ligand, which leads to the formation of a stable closed-shell anion (hydroxide in **L** and ethoxide in **H**).

A more energetically favorable regeneration mechanism from $Mn^{III}\cdots OOR$ (**O**) is available in the presence of ROH, that is,

dx.doi.org/10.1021/cs200402b |ACS Catal. 2011, 1, 1475–1486

after a certain amount of time, since the oxidation reaction started to allow for ROH production and accumulation in the catalyst pores. This regeneration pathway, discussed in section C, occurs through H transfer from the methylene C in ROH to ROO·, followed by a H transfer from the resulting radical to the framework O; the process is favored both kinetically (it has a lower activation barrier) and thermodynamically (the reaction enthalpy is less endothermic) compared with the corresponding H transfer from ethane, the latter leading to the propagation subcycle (**O** → **P** → **Q** → **O**) (Figure 12, top, solid and dashed red lines, respectively; and Table 1). The alternative regeneration mechanism (**O** → **T** → **BE** → **F**) prevents the large activation barrier required for the transformation of complex $Mn^{III}\cdots$OOR (**O**) into $Mn^{III}\cdots$OH (**L**) (Figure 12, top, green line), but requires the presence of ROH.

We have examined an alternative regeneration mechanism from complex $Mn^{III}\cdots$OR (**H**) through a unimolecular H transfer to the framework (**H** → **BE** → **F**). This process is, however, unfavorable compared with alternative reaction pathways from intermediate **H**: it has a higher activation barrier (48 k/mol) than the H transfer from ethane to the oxo ligand OR, leading to the propagation reactions (32 kJ/mol) (**H** → **I**) (Figure 12, bottom, solid and dashed lines, respectively). In terms of thermodynamics, the two alternative processes are similar: the highly exothermic nature of the aldehyde formation in the regeneration pathway is compensated by the exothermic O_2 addition in the propagation route, and the final energy is the same in both cases, −170 kJ/mol. This regeneration mechanism closes a reaction cycle (**F** → **H** → **BE** → **F**), in which initially present ROOH molecules are first decomposed by the action of Mn^{II} into H_2O and complex $Mn^{III}\cdots$OR (**H**), and the latter is then transformed into an aldehyde molecule, regenerating the Mn^{II} active sites (**F**). This subcycle transforms a hydroperoxide molecule into an aldehyde and water ($CH_3CH_2OOH \rightarrow CH_3CH(=O) + H_2O$), that is, it consumes ROOH but does not produce it; therefore, this is not a self-sustained cycle, since it can operate only in the presence of a high concentration of ROOH. Since intermediate **H** is not the final product of the propagation cycle, it does not represent the main species from which regeneration takes place, and the **H** → **BE** → **F** pathway should be considered as a side-mechanism for regeneration, but not the main one.

A similar subcycle is available from intermediate $Mn^{III}\cdots$OH (**L**) (**F** → **L** → **R** → **S** → **F**), in which a hydroperoxide molecule and a hydrocarbon are converted into two ethanol molecules ($CH_3CH_2OOH + CH_3CH_3 \rightarrow 2CH_3CH_2OH$). Again, this subcycle is not sef-sustained, since it requires hydroperoxide molecules produced elsewhere in the catalyst.

To summarize, two main regeneration mechanisms have been observed. The first involves an initial energetically costly transformation of complex $Mn^{III}\cdots$OOR (**O**) into $Mn^{III}\cdots$OH (**L**) and a subsequent H transfer from ethane to the framework, leading to the production of a ROH molecule (**O** → **L** → **R** → **S** → **F**). This pathway is kinetically hindered, and it will represent the regeneration route only at the beginning of the oxidation reaction when no oxidation products are available. At later stages of the reaction, when ROH starts to accumulate in the AFI channels produced by means of the propagation reactions, a more favorable regeneration pathway can start to take place, involving the oxidation of an alcohol molecule (ROH) into an aldehyde (R(=O)H) and producing new hydroperoxide molecules (**O** → **T** → **BE** → **F**). The occurrence of these different regeneration routes as a function of the concentration of products into the catalyst and, in turn, as a function of the reaction time explains the decrease in the alcohol-to-aldehyde ratio observed experimentally with increasing reaction time.[15] If regeneration occurs uniquely through mechanism **O** → **L** → **R** → **S** → **F**, at the beginning of the oxidation reaction, the chemical balance of the overall oxidation cycle is

$$CH_3CH_2OOH + 2CH_3CH_3 + O_2 \rightarrow 2CH_3CH_2OH + CH_3C(=O)H + H_2O \quad (1)$$

taking place through the cycle **F** → **G1/G2** → **H/M** → **I/N** → **J** → **K** → **O** → **L** → **R** → **S** → **F**. It leads to an alcohol-to-aldehyde ratio of 2:1. This cycle needs an external source of ROOH, which is provided by the propagation subcycle from $Mn^{III}\cdots$OOR (**O**) (**O** → **P** → **Q** → **O**)

$$CH_3CH_3 + O_2 \rightarrow CH_3CH_2OOH \quad (2)$$

and hence, summing eqs 1 + 2, the overall transformation is

$$3CH_3CH_3 + 2O_2 \rightarrow 2CH_3CH_2OH + CH_3C(=O)H + H_2O \quad (3)$$

When the alternative regeneration takes place through mechanism **O** → **T** → **BE** → **F**, at later stages of the reaction, the corresponding mass balance is

$$CH_3CH_3 + O_2 \rightarrow CH_3C(=O)H + H_2O \quad (4)$$

via the pathway **F** → **G1/G2** → **H/M** → **I/N** → **J** → **K** → **O** → **T** → **BE** → **F**. The net balance of the alcohol in eq 4 is zero, since once it is formed, it is converted into the aldehyde to allow for the regeneration of the catalyst. This cycle leads to an increase in the aldehyde concentration to the detriment of the alcohol, as observed experimentally. This second cycle is self-sustained, since it transforms the initial reactants, the hydrocarbon and O_2, into products and does not require an external source of ROOH (it is produced within its own cycle during the regeneration process). The overall ratio between alcohol and aldehyde in the reaction products depends on the relative rate of reactions 1 + 2 and 4 under steady-state conditions. The complexity of the overall reaction cycle makes this ratio a difficult quantity to estimate because of the large number of competitive reaction subcycles that can take place in the catalyst.

CONCLUSIONS

In the present work, we have concentrated on the regeneration mechanism by which Mn^{III} sites generated in the propagation reactions during the aerobic oxidation of alkanes by Mn-doped aluminophosphates are reduced to Mn^{II} so as to close the overall catalytic oxidation cycle. The Mn^{II} sites will then re-enter the reaction cycle by decomposing the hydroperoxide intermediates (ROOH) produced during the propagation reactions.

Our results demonstrate that two alternative regeneration mechanisms are available, and their occurrence is dictated by the composition of the reaction media, which in turn is determined by the reaction time. At the beginning of the reaction, when no alcohol molecules are present, regeneration of Mn sites in $Mn^{III}\cdots$OOR (intermediate **O**) takes place through an intramolecular H transfer from the methylene C in the peroxo ligand to give complex $Mn^{III}\cdots$OH (intermediate **L**) and an aldehyde molecule in a very exothermic step that is slow since it requires a high activation energy. The Mn sites in $Mn^{III}\cdots$OH can then be reduced by H abstraction from a hydrocarbon molecule to a

dx.doi.org/10.1021/cs200402b |ACS Catal. 2011, 1, 1475–1486

framework O, followed by a coupling between the resulting hydrocarbon radical and the OH ligand to give a molecule of ethanol and Mn^{II} sites. At later stages of the reaction, when the alcohol molecules (primary oxidation product) are present in the reaction mixture, the activated nature of the alcohol provides a more energetically favored regeneration pathway from $Mn^{III}\cdots$ OOR; H-abstraction takes place from the methylene C in the alcohol to the peroxo ligand to give ROOH and a hydroxyethyl radical $CH_3CH\cdot OH$, from which reduction of Mn occurs by a second H abstraction from the hydroxy group, yielding an aldehyde molecule and Mn^{II} sites.

The operation of these two regeneration mechanisms and their occurrence at different times during the hydrocarbon oxidation explains the variation of the alcohol-to-aldehyde ratio experimentally observed as a function of the reaction time: the initial regeneration mechanism leads to a higher concentration of alcohol products, and the second route produces aldehyde to the detriment of the alcohol, suggesting a decrease of the alcohol-to-aldehyde ratio with increasing the reaction time, in good agreement with the experimental observations.

■ ASSOCIATED CONTENT

Supporting Information. Additional reaction schemes, energy profiles, molecular structures and spin density plots of several intermediates. This material is available free of charge via the Internet at http://pubs.acs.org/.

■ AUTHOR INFORMATION

Corresponding Author
*E-mail: (L.G.-H.) lhortiguela@icp.csic.es, (F.C.) f.cora@ucl.ac.uk.

■ ACKNOWLEDGMENT

L.G.-H. acknowledges funding from EPSRC (Grant EP/D504872). We are grateful to Sir John Meurig Thomas, Gopinathan Sankar, and Claudio M. Zicovich-Wilson for helpful discussions. The authors acknowledge the use of the UCL Legion High Performance Computing Facility and associated support services in the completion of this work.

■ REFERENCES

(1) Wilson, S. T.; Lok, B. M.; Flanigen, E. M. US Patent 4310440, 1982.
(2) Raja, R.; Thomas, J. M. *Chem. Commun.* **1998**, 1841–1842.
(3) Saadoune, I.; Corà, F.; Alfredsson, M.; Catlow, C. R. A. *J. Phys. Chem. B* **2003**, *107*, 3012–3018.
(4) Corà, F.; Sankar, G.; Catlow, C. R. A.; Thomas, J. M. *Chem. Commun.* **2002**, 734–735.
(5) Thomas, J. M. *Angew. Chem., Int. Ed.* **1999**, *38*, 3588–3628.
(6) Arends, I. W. C. E.; Sheldon, R. A.; Wallau, M.; Schuchardt, U. *Angew. Chem., Int. Ed. Engl.* **1997**, *36*, 1144–1163.
(7) Hartmann, M.; Ernst, S. *Angew. Chem., Int. Ed.* **2000**, *39*, 888–890.
(8) Thomas, J. M.; Raja, R.; Sankar, G.; Bell, R. *Nature* **1999**, *298*, 227–230.
(9) Modén, B.; Oliviero, L.; Dakka, J.; Santiesteban, J. G.; Iglesia, E. *J. Phys. Chem. B* **2004**, *108*, 5552–5563.
(10) Modén, B.; Zhan, B.-Z.; Dakka, J.; Santiesteban, J. G.; Iglesia, E. *J. Phys. Chem. C* **2007**, *111*, 1402–1411.
(11) Raja, R.; Sankar, G.; Thomas, J. M. *Angew. Chem., Int. Ed.* **2000**, *39*, 2313–2316.
(12) Vanoppen, D. L.; De Vos, D. E.; Genet, M. J.; Rouxhet, P. G.; Jacobs, P. A. *Angew. Chem., Int. Ed. Engl.* **1995**, *34*, 560–563.
(13) Luna, F. J.; Ukawa, S. E.; Wallau, M.; Schuchardt, U. *J. Mol. Catal. A, Chem.* **1997**, *117*, 405–411.
(14) Raja, R.; Sankar, G.; Thomas, J. M. *J. Am. Chem. Soc.* **1999**, *121*, 11926–11927.
(15) Modén, B.; Zhan, B.-Z.; Dakka, J.; Santiesteban, J. G.; Iglesia, E. *J. Catal.* **2006**, *239*, 390–401.
(16) Concepción, P.; Corma, A.; López-Nieto, J. M.; Pérez-Pariente, J. *App. Catal., A* **1996**, *143*, 17–28.
(17) Zhou, L.; Xu, J.; Chen, C.; Wang, F.; Li, X. *J. Porous Mater.* **2008**, *15*, 7–12.
(18) Dugal, M.; Sankar, G.; Raja, R.; Thomas, J. M. *Angew. Chem., Int. Ed.* **2000**, *39*, 2310–2313.
(19) Raja, R.; Sankar, G.; Thomas, J. M. *Chem. Commun.* **1999**, 829–830.
(20) Raja, R.; Thomas, J. M.; Dreyer, V. *Catal. Lett.* **2006**, *110*, 179–183.
(21) Raja, R.; Thomas, J. M.; Sankar, G. *Chem. Commun.* **1999**, 525–526.
(22) Gómez-Hortigüela, L.; Corà, F.; Sankar, G.; Zicovich-Wilson, C. M.; Catlow, C. R. A. *Chem.—Eur. J.* **2010**, *16*, 13638–13645.
(23) Gómez-Hortigüela, L.; Corà, F.; Catlow, C. R. A. *ACS Catal.* **2011**, *1*, 18–28.
(24) Gómez-Hortigüela, L.; Corà, F.; Catlow, C. R. A. *ACS Catal.* **2011**, *1*, 945–955.
(25) Gómez-Hortigüela, L.; Corà, F.; Catlow, C. R. A. *ACS Catal.*; DOI: cs-201100401f.
(26) Dovesi, R.; Saunders, V. R.; Roetti, C.; Orlando, R.; Zicovich-Wilson, C. M.; Pascale, F.; Civalleri, B.; Doll, K.; Harrison, N. M.; Bush, I. J.; D'Arco, Ph.; Llunell, M. *CRYSTAL06*; University of Torino: Torino, 2006.
(27) Grimme, S. *J. Comput. Chem.* **2006**, *27*, 1787–1799.
(28) Ugliengo, P.; Zicovich-Wilson, C. M.; Tosoni, S.; Civalleri, B. *J. Mater. Chem.* **2009**, *19*, 2564–2572.